Bioorganic Chemistry 114 (2021) 105037

Contents lists available at ScienceDirect

Bioorganic Chemistry

journal homepage: www.elsevier.com/locate/bioorg

Synthesis and evaluation of the anti-inflammatory activity of novel 8-quinolinesulfonamide derivatives as TLR4/MD-2 inhibitors with efficacy in adjuvant-induced arthritis

Tongtong Liu, Siqi Xing, Jiyu Du, Min Wang, Jianfei Han, Zeng Li *

Inflammation and Immune Mediated Diseases Laboratory of Anhui Province, Anhui Institute of Innovative Drugs, School of Pharmacy, Anhui Medical University, Hefei 230032, China

ARTICLE INFO

Keywords:
8-Quinolinesulfonamide derivatives
Anti-inflammatory
3l
TLR4/MD-2
Adjuvant induced arthritis

ABSTRACT

In this study, a series of 8-quinolinesulfonamide derivatives was synthesized, and their anti-inflammatory activity was evaluated. Among them, compound **3l** was found to be the best anti-inflammatory agent, with IC_{50} values of 2.61 ± 0.39, 9.74 ± 0.85, and 12.71 ± 1.34 μM against NO, TNF-α and IL-1β production respectively. And **3l** could significantly prevent lipopolysaccharide (LPS)-induced expression of inflammatory mediators (iNOS and COX-2). Molecule docking results showed that **3l** could bind to the LPS binding site of toll-like receptor 4 (TLR4)/MD-2, and **3l** was then identified as TLR4/MD-2 inhibitor by co-immunoprecipitation (co-IP) and cellular thermal shift assay (CTESA). Preliminary mechanism studies indicated that **3l** could prevent TLR4 from being activated by disrupting TLR4/MD-2 heterodimerization and TLR4 homodimerization, thereby blocking the activation of the NF-κB/MAPK signaling pathway. Furthermore, observation of rat foot swelling, joint pathology and serum inflammatory cytokine levels proved that compound **3l** had a significant therapeutic effect on adjuvant-induced arthritis (AIA) in rats *in vivo*. These results indicated that compound **3l** is a potential anti-inflammatory agent, from which more effective anti-inflammatory drugs could be developed.

1. Introduction

Inflammation is a biological protective response of the organism against injury or infection [1,2]. Disorder in tissues may cause inflammation, such as joint disease, cancer, and heart failure [3–6]. However, inflammation can be reduced by inhibiting the production of inflammatory factors (e.g., TNF-α, IL-1β, IL-6, and NO) [7–9]. The classic drugs currently used for the treatment of inflammation are nonsteroidal anti-inflammatory drugs, such as aspirin, but these drugs can cause some adverse reactions [10,11]. Therefore, new anti-inflammatory drugs must be discovered and developed.

Toll-like receptors (TLRs) are a class of proteins that play a key role in the innate immune system [12]. Among them, TLR4 has been shown to be related to various inflammatory diseases and can regulate the immune homeostasis of the human system; thus, it is considered the most influential target [13,14]. TLR4, along with its accessory protein MD-2, is dimerized under LPS stimulation, which promotes the interaction between the downstream effector myeloid differentiation factor 88 and dimerized TLR4/MD-2 to control the cascade of NF-κB and MAPK that results in the activation of downstream cytokines, such as NO, TNF-α, and IL-1β [12,15–18]. Several studies have shown that various compounds that act as TLR4/MD-2 inhibitors can exert anti-inflammatory effects by preventing the combination of TLR4 and MD-2 [19–21]. Thus, inhibiting TLR4/MD-2 activation can effectively reduce the expression of TLR4-related inflammatory cytokines to reduce inflammation.

Most quinoline derivatives have good anti-inflammatory activity (Fig. 1) [22–26]. Hence, the quinoline scaffold can be used as a key matrix structure to design drugs with a better anti-inflammatory activity. In addition, sulfonamide groups play an important role in anti-inflammatory drugs. Certain agents with a benzenesulfonamide structure, such as nimesulide, celecoxib, and parecoxib, are commonly used in clinical settings to reduce inflammation (Fig. 1) [27–29]. In this study, we introduced sulfonamide groups into the quinoline ring to synthesize a series of 8-quinolinesulfonamide derivatives (Fig. 1). We evaluated derivatives anti-inflammatory activities *in vitro*. The title 8-quinolinesulfonamide derivative optimized was further evaluated to elucidate their potential mechanism of action and used to explore ameliorate

* Corresponding author.
E-mail address: lizeng@ahmu.edu.cn (Z. Li).

https://doi.org/10.1016/j.bioorg.2021.105037
Received 16 April 2021; Received in revised form 24 May 2021; Accepted 28 May 2021
Available online 31 May 2021

inflammation in a AIA mouse model.

2. Results and discussion

2.1. Chemistry

The synthesis route of 8-quinolinesulfonamide derivatives is illustrated in Scheme 1. A series of compounds, **3a**–**3n**, were obtained by reacting various substituents of aniline and 8-quinolinesulfonyl chloride and triethylamine in dichloromethane at room temperature.

2.2. ADMET predictions for compounds

The absorption, distribution, metabolism, excretion, and toxicity (ADMET) of compounds **3a**–**3n** were predicted using the Discovery Studio 2017 (DS 2017) software [30,31]. The results are depicted in the 2D graphs of ADMET PSA 2D and ADMET AlogP98. Compound **3a** had poor solubility at 25 °C (solubility level of 3), whereas compounds **3b**–**3n** had good solubility at this temperature (solubility level of 1 or 2) (Fig. 2 and Table 1). All compounds were within the 95% and 99% confidence intervals of blood–brain barrier (BBB) penetration and had good HIA (absorption level of 0). Moreover, compounds **3a**–**3n** were likely to bind to plasma proteins (PPB# prediction was true). Results showed that these compounds were non-cytochrome P450 2D6 inhibitors (CYP2D6# prediction was false). The druggability and safety of the compounds were initially evaluated through ADMET predictions. Subsequently, the anti-inflammatory activity of the compounds was studied.

2.3. Inhibition of NO production and inflammatory factors in LPS-induced RAW264.7 cells

A series of synthetic 8-quinolinesulfonamide derivatives were determined and their cytotoxicity in macrophage RAW264.7 cells was evaluated by MTT assay to prevent the toxicity of compounds **3a–3n** to the cells from interfering with the analysis of experimental results. As shown in Table 2, compared with positive drug indomethacin, compounds **3a** and **3h** displayed weak cytotoxicity, whereas the other compounds showed low toxicity.

LPS is a common immunostimulator that can stimulate RAW264.7 cells to induce and secrete NO, IL-1β, TNF-α, and other inflammatory factors [2,32,33]. Overproduction of NO and pro-inflammatory factors is closely related to inflammatory diseases [2,34,35]. Thus, the anti-inflammatory activity of all compounds synthesized herein was

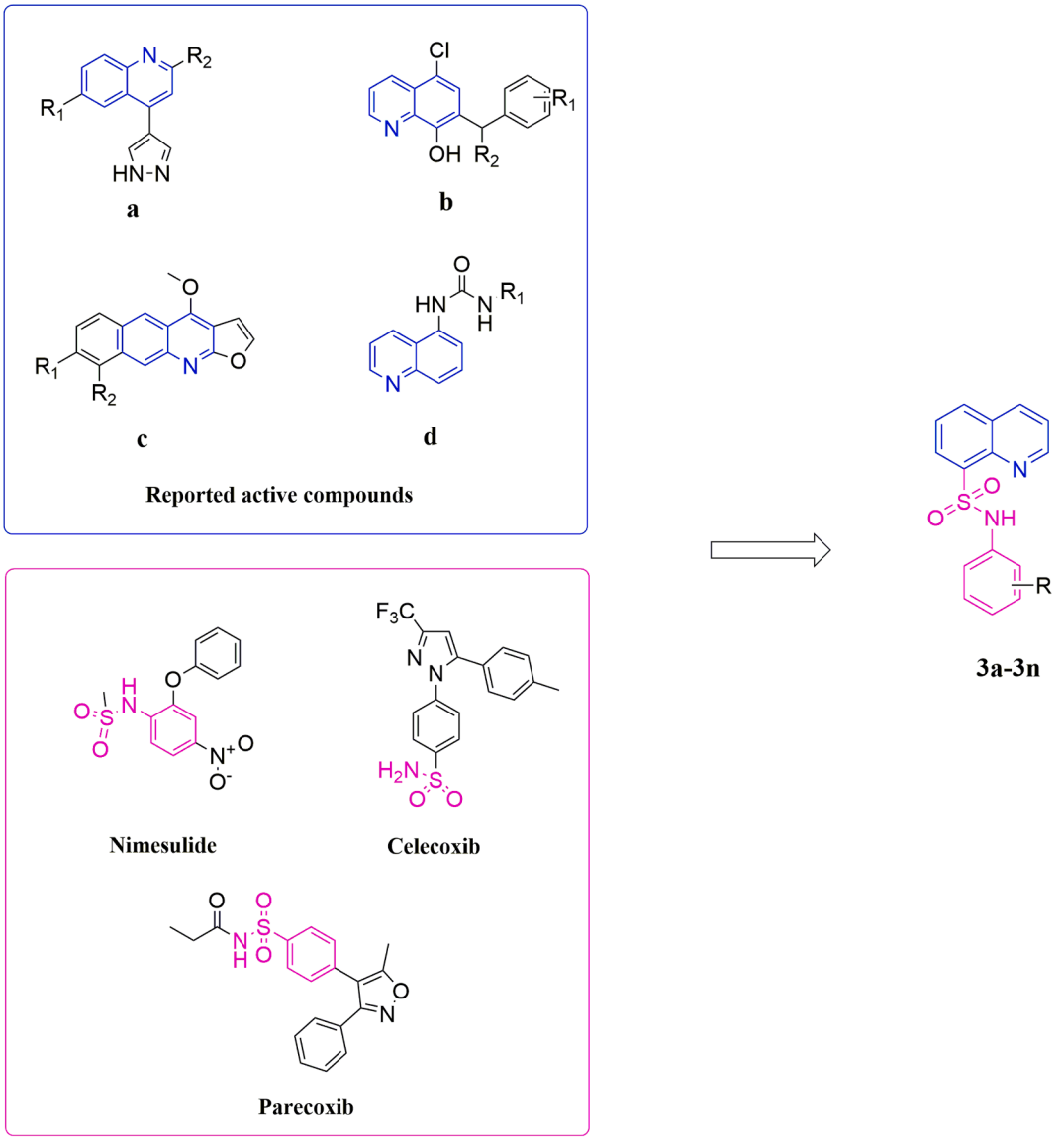

Fig. 1. A strategy for designing an anti-inflammatory drug.

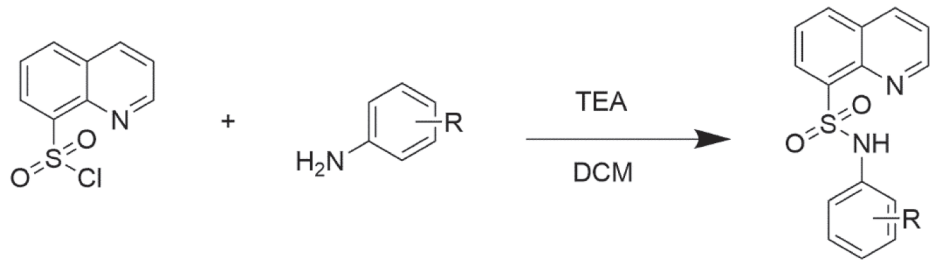

1 **2** **3a-3n**

Compd	R	Compd	R
3a	H	**3h**	2-F
3b	2-CH_3	**3i**	3-F
3c	3-CH_3	**3j**	4-F
3d	4-CH_3	**3k**	3,4-F
3e	2-OCH_3	**3l**	4-CF_3
3f	3-OCH_3	**3m**	4-OCF_3
3g	4-OCH_3	**3n**	3-Cl

Scheme 1. Synthesis of 8-quinolinesulfonamide derivatives **3a**–**3n**. Reagents and conditions: dichloromethane, triethylamine, ethanol, room temperature, 3–10 h. [a] Yield of the compound obtained.

evaluated. A nonsteroidal anti-inflammatory drug, indomethacin, was selected as a positive control. RAW264.7 cells were incultured with different concentrations of the compounds (100, 60, 40, 20, 10, 5, 2.5, 1.25 and 0.6725 μM) for 1 h and stimulated by LPS for 24 h. The inhibitory effect of the compounds on NO production in the cell supernatant was detected using a NO content detection kit (Table 3).

Analysis of structure–activity relationship revealed that the introduction of different substituents of the phenyl ring expressed different degrees of anti-inflammatory activity. When the phenyl ring had no substituent (**3a**), the anti-inflammatory activity of the compound was weaker than that of the positive drug indomethacin. Furthermore, compound **3k** exhibited poor anti-inflammatory activity, much less than that of the positive drug, which may be the cause of steric hindrance. However, the introduction of a single substituent on the phenyl ring of the other compounds evidently enhanced their anti-inflammatory activity and was superior to positive drug. Among these compounds, that with the CF_3 group (i.e., compound **3l**) had the best inhibitory activity, which is about 16 times stronger than indomethacin. Moreover, the electronegativity of the substituents on the phenyl ring was strongly related to the inhibitory activity. When a strong electron withdrawing group (F or Cl) was introduced into the phenyl ring, the inhibitory activity against NO production was evidently enhanced, and its activity was related to the position of the substituent on the phenyl ring. The introduction of substituents at the *C*2, C3, and C4 positions of phenyl

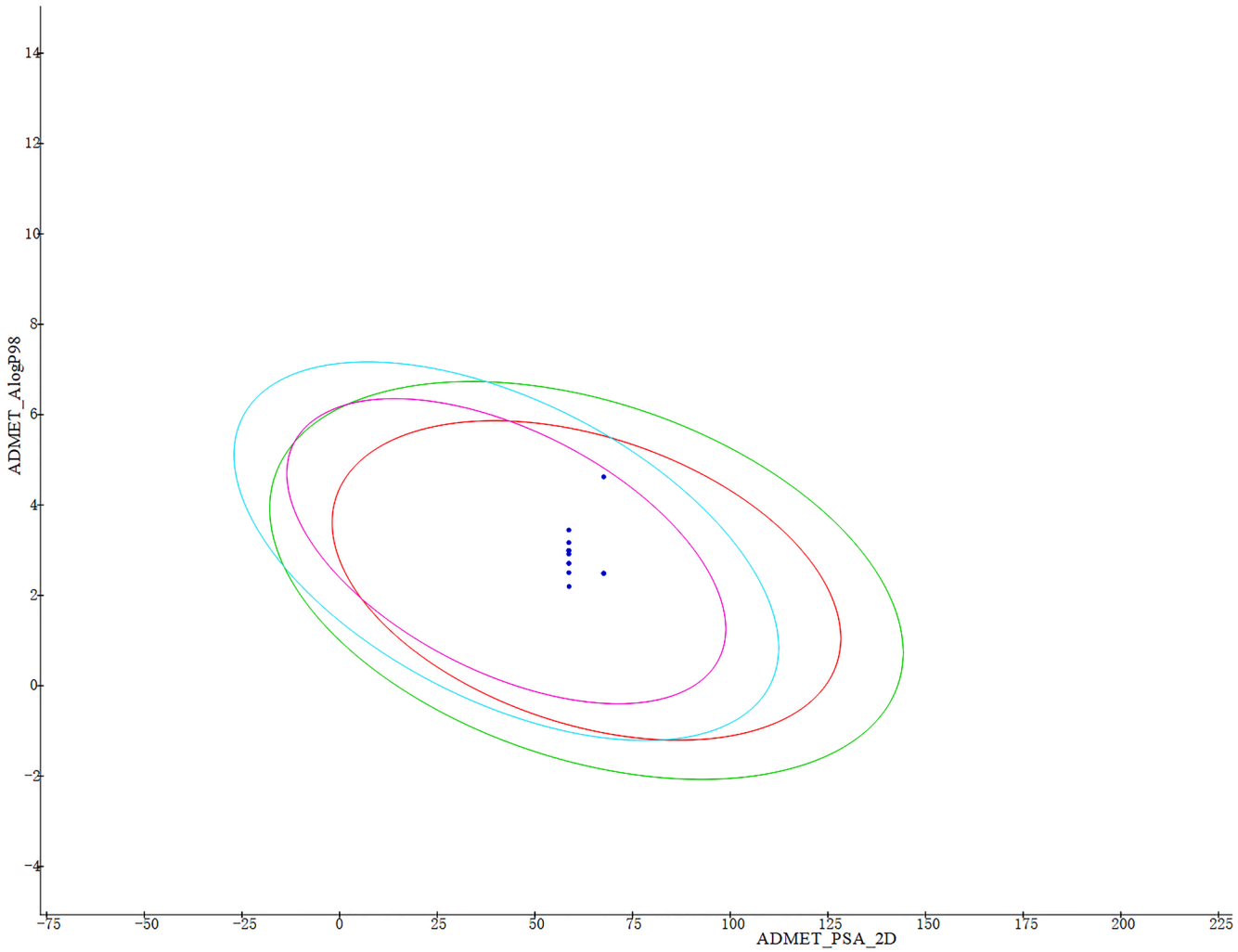

Fig. 2. Regression of ADMET_PSA_2D and ADMET_AlogP98. Red represents the 95% confidence interval of HIA, and green denotes the 99% confidence interval of HIA. Pink indicates the 95% confidence interval of BBB, and the sky blue ellipse signifies the 99% confidence interval of BBB. All compounds are within the confidence interval. (For interpretation of the references to colour in this figure legend, the reader is referred to the web version of this article.)

rings gradually decreased the inhibitory activities of the derivatives against NO, such as compounds **3h**, **3i**, and **3j**. Interestingly, in contrast to the electron-withdrawing group, the activity of the electron-donating group at the C4 position (compound **3d**) was better than that at the C2 (compound **3b**) and C3 (compound **3c**) positions. This trend was also observed in compounds **3e**, **3f**, and **3g**. Moreover, the effectiveness of the compound with a F substituent was better than that of the derivative with a Cl substituent in the 3 position of the phenyl ring, which also surpassing of indomethacin.

In this study, the inhibitory effect of the compounds on the production of IL-1β and TNF-α was detected via ELISA to evaluate further their anti-inflammatory activity. As shown in Table 3, compound **3l** had the best inhibitory effect on the secretion of inflammatory factors NO, IL-1β, and TNF-α in RAW264.7 cells.

NO production is mediated by COX-2 and iNOS. When inflammatory cells are stimulated by LPS, COX-2 and iNOS are overexpressed [1,36,37]. The effects of compound **3l** on the expression of pro-inflammatory factors in LPS-treated RAW264.7 cells were analyzed via Western blot. Results showed that compound **3l** could reduce the expression of iNOS and COX-2 in a concentration-dependent manner (Fig. 3).

2.4. Reverse virtual screening and molecular docking

Reverse virtual screening is used to find and identify potential targets from receptors through known ligand structures via three methods, namely, shape screening, pharmacophore screening, and reverse docking [38,39]. In the present study, reverse virtual screening was applied to validate that the 8-quinolinesulfonamide derivative compound **3l** had a good binding relationship with TLR4/MD-2 protein (PDB:3FXI) (**Fig. S1**). Thus, TLR4/MD-2 was considered as a possible target of compound **3l**. The results were further analyzed via molecule docking by using the CDOCKER program in Discovery Studio 2017 soft. As shown in Fig. 4, compound **3l** had a good binding in the LPS-binding pocket of the TLR4/MD-2 complex and formed an interaction with the amino acids of the TLR4 protein (Ser183, Ala58, Asp181, Asn156, and Val134) and the amino acids of the MD-2 protein (Leu108, Arg106, and Glu111). Therefore, we speculated that compound **3l** could be used as a TLR4/MD-2 inhibitor to exert anti-inflammatory effects.

2.5. Effects of compound *3l* on TLR4/MD-2 complex

Given that molecular docking established a direct relationship between compound **3l** and the active site of the TLR4/MD-2 complex, we further confirmed that TLR4/MD-2 as the target of compound **3l** by co-IP, the result showed that **3l** significantly inhibited dimerization of the TLR4/MD-2 complex (Fig. 5).

TLR4/MD-2 heterodimerization in the presence of LPS results in homodimerization of TLR4, inducing the release of pro-inflammatory

Table 1
ADMET predictions for compounds **3a-3n.**

compd	Absorption level[a]	BBB level[b]	Solubility level[c]	CYP2D6[d]	PPB[e]	AlogP98[f]	PSA 2D[g]
3a	0	2	3	false	true	2.709	58.672
3b	0	2	2	false	true	2.709	58.672
3c	0	2	2	false	true	2.914	58.672
3d	0	2	2	false	true	3.168	58.672
3e	0	2	2	false	true	2.487	67.602
3f	0	2	2	false	true	2.99	67.602
3g	0	2	2	false	true	2.503	67.602
3h	0	2	2	false	true	2.99	58.672
3i	0	2	2	false	true	2.487	58.672
3j	0	2	2	false	true	2.99	58.672
3k	0	2	2	false	true	2.197	58.735
3l	0	2	2	false	true	3.446	58.672
3m	0	1	1	false	true	2.487	67.602
3n	0	2	2	false	true	4.623	58.672

[a] Absorption (level 0 means good).

[b] Distribution: Aqueous solubility (level 1 means very good, level 2 means moderate).

[c] Distribution: Blood–brain barrier penetration (level 1 means very good, level 2 means moderate, [k] level 3 means poor).

[d] Metabolism.

[e] Excretion.

[f] Predicted octanol/water.

[g] Two-dimensional.

Table 2
Cytotoxicity of the compounds.

compd	RAW264.7 cells IC_{50} (μM)[a]	compd	RAW264.7 cells IC_{50} (μM)[a]
3a	90.26 ± 1.7	**3i**	>100
3b	>100	**3j**	>100
3c	>100	**3k**	>100
3d	>100	**3l**	>100
3e	>100	**3m**	>100
3f	>100	**3n**	>100
3g	>100	Indomethacin	93.88 ± 2.6
3h	90.01 ± 1.9	Control	>100

[a] Concentration of the compounds at 50% survival of RAW264.7 cells. IC_{50} values are calculated from the average of three experiments (mean ± SD).

Table 3
Inhibition by the compounds of the IC_{50} value produced by inflammatory factors.

Compound	NO inhibition IC50 (μM)[a]	IL-1β inhibition IC50 (μM)[b]	TNF-α inhibition IC50 (μM)[c]
3a	47.96 ± 0.58	46.62 ± 1.53	37.18 ± 2.57
3b	31.39 ± 0.41	28.91 ± 0.51	40.08 ± 1.24
3c	22.94 ± 1.44	14.79 ± 0.82	14.53 ± 1.61
3d	18.06 ± 0.46	14.67 ± 0.93	36.13 ± 0.37
3e	31.07 ± 1.17	24.97 ± 0.58	45.25 ± 1.22
3f	19.98 ± 0.71	23.07 ± 0.49	20.89 ± 0.77
3g	16.78 ± 0.30	30.05 ± 1.27	40.71 ± 1.62
3h	5.47 ± 0.72	12.24 ± 1.33	26.69 ± 1.05
3i	17.92 ± 0.32	49.30 ± 0.33	33.34 ± 0.47
3j	24.81 ± 0.44	39.63 ± 0.21	47.65 ± 0.94
3k	> 100	> 100	> 100
3l	2.61 ± 0.39	9.74 ± 0.85	12.71 ± 1.34
3m	9.76 ± 0.66	10.78 ± 0.96	17.32 ± 0.49
3n	25.41 ± 0.53	54.45 ± 0.38	28.74 ± 0.79
Indomethacin	34.99 ± 0.26	36.15 ± 0.62	40.96 ± 0.63

[a] Concentration of the compounds when 50% NO was produced in LPS-stimulated RAW264.7 cells. IC_{50} values are calculated from the average of three experiments (mean ± SD).

[b] Concentration of the compounds when 50% IL-1β was produced in LPS-stimulated RAW264.7 cells. IC_{50} values are calculated from the average of three experiments (mean ± SD).

[c] Concentration of the compounds when 50% TNF-α was produced in LPS-stimulated RAW264.7 cells. IC_{50} values are calculated from the average of three experiments (mean ± SD).

cytokines, such as NO, IL-6, and TNF-α [16,19,40], thus the interaction between compound **3l** and TLR4 was further analyzed by CETSA and immunoprecipitation. CETSA is a biophysical technique for monitoring ligand–potein interactions [41,42]. In the CETSA method, cells or cell extract samples are heated at different temperatures to evaluate the compound's effect on the thermal stability of protein, thereby providing quantitative evidence for compound–protein interactions [43,44]. Results showed that the TLR4 protein collected from RAW264.7 cells co-cultured with compound **3l** had a better stability than the cells incubated in the absence of this compound at 50 °C and 55 °C, indicating that TLR4 interacted with this compound (Fig. 6). To evaluate the effect of **3l** on TLR4 dimerization, HEK293T cells were co-transfected with TLR4-HA acid and TLR4-Flag plasmids for 24 h, and then TLR4-Flag and TLR4-HA acid complexes were detected by co-IP. Compound **3l** substantially reduced the TLR4-Flag of TLR4-HA, indicating that this compound disrupted the TLR4 dimerization associated with LPS (Fig. 7).

2.6. Inhibition of LPS-induced NF-κB/MAPK signaling activation

When the TLR4/MD-2 complex is stimulated by LPS, a series of signal cascades are initiated to activate the NF-κB and MAPK signaling pathways [15,21,45]. Accordingly, the effect of the compound on the expression of related proteins in the NF-κB and MAPK signaling pathways were analyzed.

Compound **3l** inhibited the phosphorylation and degradation of IκB

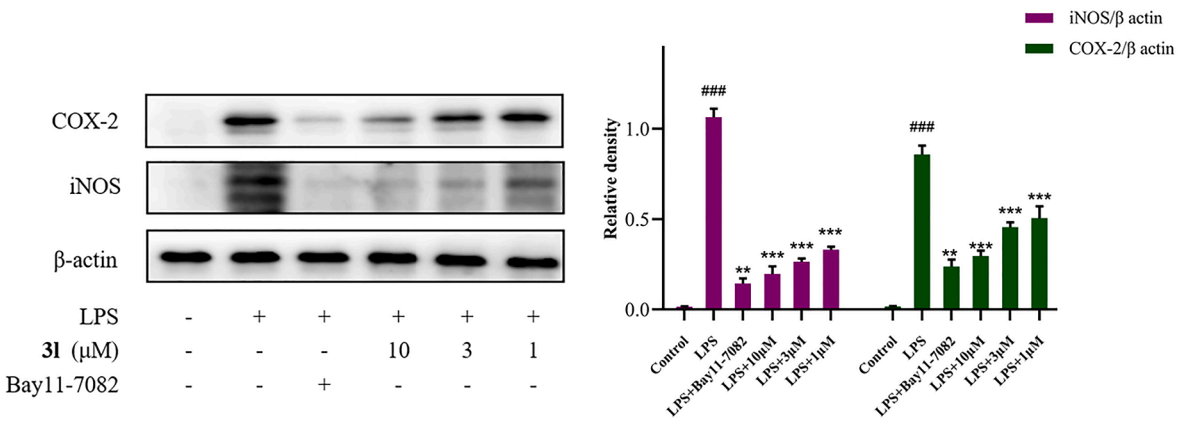

Fig. 3. Effects of compound **3l** on the expression of related inflammatory proteins. RAW264.7 cells were incubated with different concentrations of compound **3l** and the positive drug (1, 3, and 10 μM) Bay11-7082 for 1 h. The cells were then stimulated by LPS for 24 h. The effects of compound **3l** on iNOS and COX-2 were analyzed by Western blot. The results were showed as means ± SD (n = 3) of at least three independent experiments. $^{\#\#\#}p < 0.0001$ compared with control, $^{**}p < 0.001$, $^{***}p < 0.001$ compared with LPS-stimulated cells.

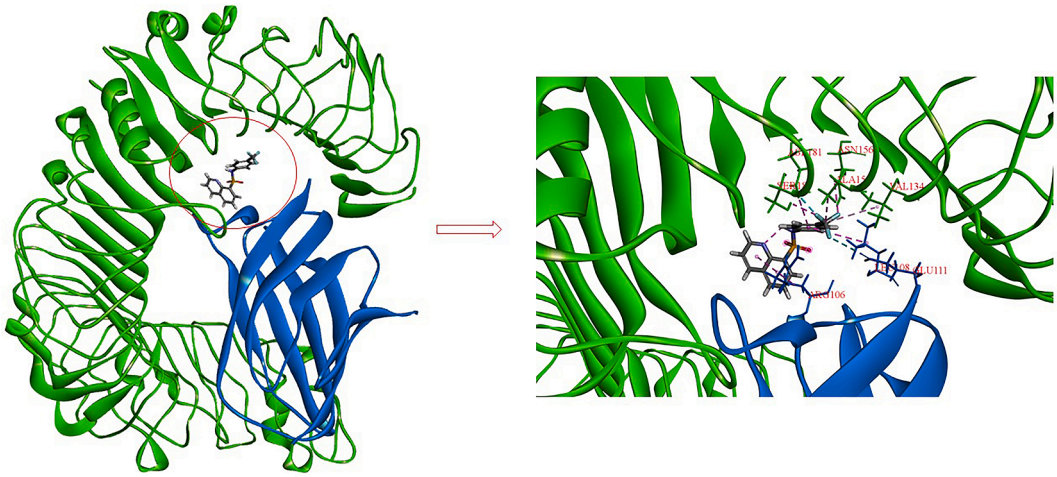

Fig. 4. Compound **3l** bound to the LPS-binding pocket of the TLR4/MD-2 complex (PDB: 3FXI). Green denotes the TLR4 protein, and blue indicates the MD-2 protein. (For interpretation of the references to colour in this figure legend, the reader is referred to the web version of this article.)

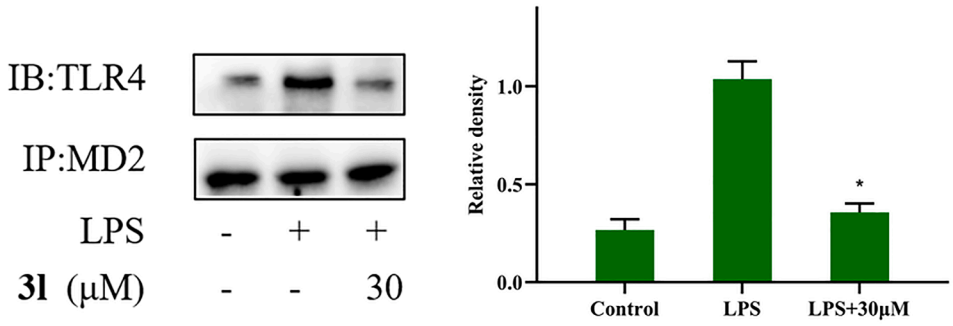

Fig. 5. Co-immunoprecipitation showing effect of compound **3l** pretreatment the formation of TLR4/MD-2 complex in RAW264.7 cells exposed to LPS. The results were showed as means ± SD (n = 3) of at least three independent experiments. *p < 0.01 compared with LPS-stimulated cells.

to block the activation of IκB kinase (Fig. 8**A**). Moreover, it inhibited the phosphorylation of P65 in a concentration-dependent manner and prevented the translocation of NF-κB P65 from the cytoplasm to the nucleus. RAW264.7 cells were stimulated to activate the MAPK signaling pathway, leading to considerable phosphorylation of MAPK (P38, JNK, and ERK). As suggested in Fig. 8**B**, compound **3l** (1, 3, and 10 μM) could also inhibit LPS-induced P38, JNK, and ERK phosphorylation in a concentration-dependent manner.

2.7. *Anti-inflammatory activity of compound **3l** in vivo*

The anti-inflammatory activity of compound **3l** *in vivo* was confirmed by using compound **3l** (10 and 30 mg/kg) and a positive drug (10 mg/kg) used to treat the rat adjuvant-induced arthritis (AIA) model.

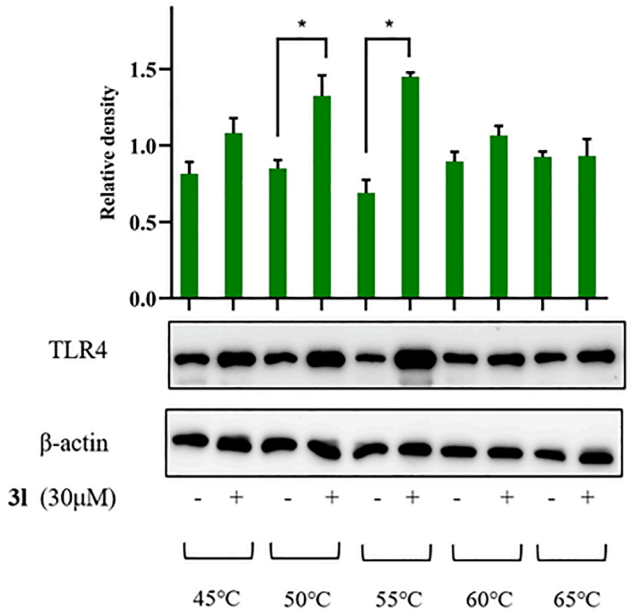

Fig. 6. Interaction between of compound **3l** and TLR4. RAW264.7 cells were treated with **3l** for 12 h, and then the expression of TLR4 protein at different temperatures (45 °C, 50 °C, 55 °C, 60 °C and 65 °C) was detected. The results were showed as means ± SD (n = 3) of at least three independent experiments. *p < 0.01 compared with LPS-stimulated cells.

Compared with the model group, the drug group reduced the swelling of the rats' feet in a concentration-dependent manner (Fig. 9**A and B**). On day 24, 30 mg/kg of compound **3l** significantly decreased the arthritis index (Fig. 9**C**). Compared with that in the model group, body weight in the drug group improved at doses of ≥ 10 mg/kg (Fig. 9**D**).

Subsequently, histopathological section of rat knee joints were stained with hematoxylin and eosin (HE) to investigate the effects of compound **3l** on pathological changes in AIA rats. As depicted in Fig. 10, the model group showed obvious synovial cell proliferation, inflammatory cell infiltration and pannus formation. These symptoms in AIA rats treated with compound **3l** were alleviated in a dose-dependent manner (Fig. 10).

Fuethermore, the ELISA method was used to detect inflammatory factors in the serum of AIA rats. In the results, compared with those in the normal group, the levels of IL-1β, and TNF-α in the model group remarkably increased. However, compound **3l** could reduce the inflammatory factors in the serum of rats in a dose-dependent manner. Similarly, indomethacin had an inhibitory effect on the production of inflammatory factors (Fig. 11).

3. Conclusions

This study aimed to discover novel agents with anti-inflammatory activity. A series of 8-quinolinesulfonamide derivatives were synthesized. Preliminary evaluation results of the anti-inflammatory activity of these derivatives revealed that most of them had good inhibitory activity against NO, IL-1β, and TNF-α. Analysis of the structure–activity relationship of these compounds showed that those with a single substituent on the phenyl ring had enhanced anti-inflammatory activity. Among these compounds, compound **3l** had the best anti-inflammatory activity and could significantly suppress the expression levels of iNOS and COX-2. The potential target (TLR4/MD-2) of compound **3l** was obtained through reverse screening, and confirmed by molecular docking, co-IP and CTESA. Preliminary results of mechanism studies indicated that compound **3l** could block the activation of NF-κB/MAPK signaling pathway in a concentration-dependent manner by disrupting TLR4/MD-2 dimerization. In addition, according to in *vivo* studies, compared with the model group, the treatment group (compound **3l**) effectively reduced inflammation in the AIA rat model. These findings indicated that compound **3l** has a great potential for the treatment of inflammation. We are investigating this compound in greater detail to understand further its anti-inflammatory activity.

4. Experimental section

4.1. Chemistry

Unless otherwise specified, aniline with various substituents, triethylamine, ethanol, and various solvents used in this experiment were obtained from commercial sources and did not require further purification. The reaction was monitored by thin-layer chromatography (TLC) on a silica gel plate (HSGF254 Yantai Jiangyou Silica Gel Development Co., Ltd., China) by using the solvents petroleum ether and ethyl acetate. The compounds were detected via high-resolution mass spectrometry. Proton nuclear magnetic resonance spectrum and carbon nuclear magnetic resonance spectrum were measured at 400 and 101 MHz, respectively. The reaction mixture through CombiFlash NextGen 300+ silica gel column (Teledyne ISCO, USA, Silica gel: 200–300 mesh) for purification to obtain the target product.

4.2. General procedure for the synthesis of compounds *3a–3n*

According to the reported method [46], 8-quinolinesulfonyl chloride

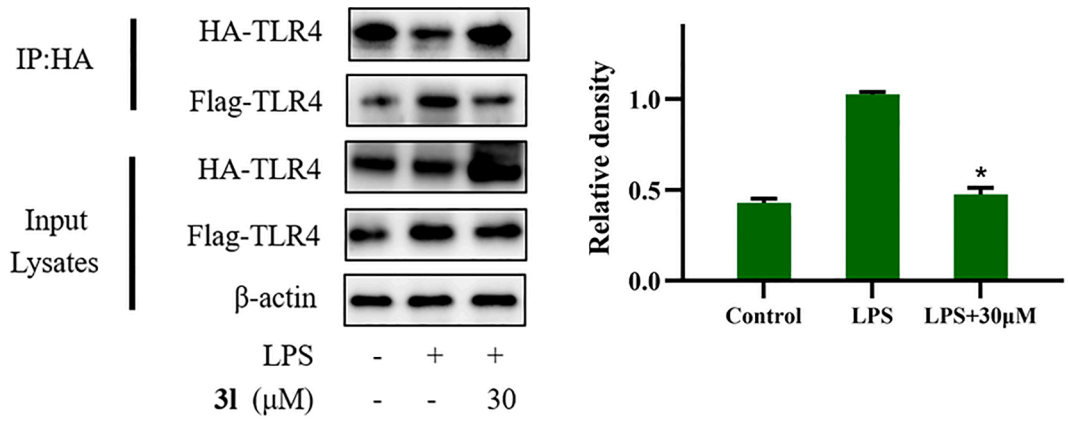

Fig. 7. Co-immunoprecipitation analysis the destructive effects of compound **3l** on TLR4 dimerization. HEK293T cells were co-transfected with TLR4-hyaluronic acid and TLR-Flag, the sampled proteins were immunoprecipitated using anti-HA magnetic beads. The results were showed as means ± SD (n = 3) of at least three independent experiments. *p < 0.01 compared with LPS-stimulated cells.

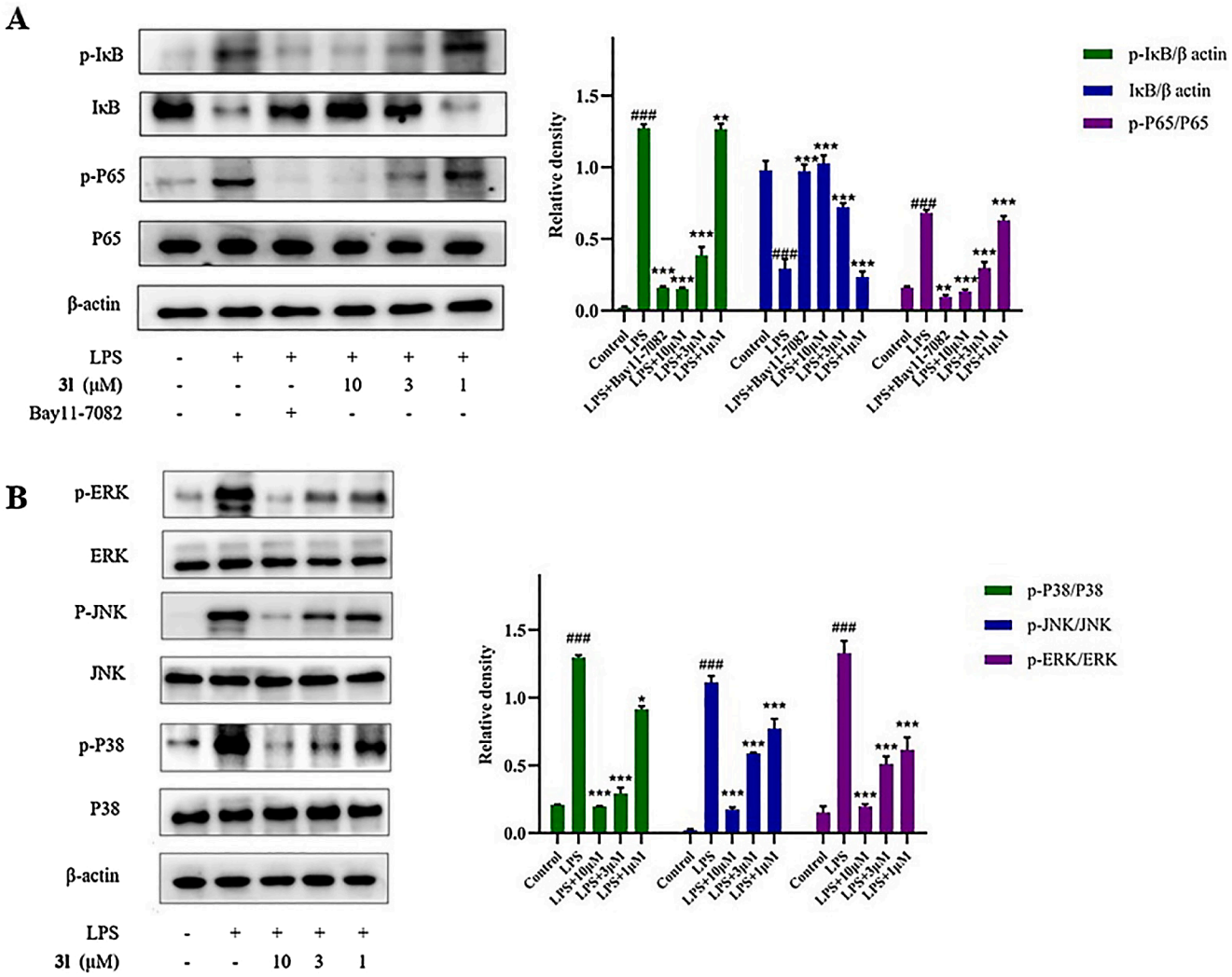

Fig. 8. Compound **3l** inhibits LPS-induced activation of NF-κB signaling pathway and MAPK signaling pathway. (A) Compound **3l** inhibites NF-κB signaling pathway in RAW 264.7 cells. (B) Compound **3l** inhibites MAPK signaling pathway in RAW 264.7 cells. RAW264.7 cells were cultured with different concentrations of compound **3l** (1, 3, and 10 μM) for 1 h. Subsequently, LPS was added for 24 h. The results were showed as means ± SD (n = 3) of at least three independent experiments. $^{###}p < 0.0001$ compared with control, $^{*}p < 0.01$, $^{**}p < 0.001$, $^{***}p < 0.0001$ compared with LPS-stimulated cells.

(227 mg, 1.0 equivalent, 1 mM) and aniline with various substituents (2.0 equivalent, 2 mM) were stirred in dichloromethane solvent for 15 min, and then triethylamine was added dropwise (101 mg, 2.0 equivalents, 2 mM). The reaction was stirred for 3–10 h at room temperature. After the TLC detection reaction was completed, the dichloromethane was removed by evaporation to obtain a reaction mixture. The mixture was purified by silica gel column chromatography using a mixture of ethyl acetate and petroleum ether to obtain the target compounds (**3a**–**3n**).

N-phenylquinoline-8-sulfonamide **(3a)** [47]. Yield: 68%. ^{1}H NMR (500 MHz, DMSO) δ 10.16 (s, 1H), 9.19 (dd, J = 4.1, 1.5 Hz, 1H), 8.53–8.45 (m, 1H), 8.42 (d, J = 7.3 Hz, 1H), 8.23 (d, J = 8.1 Hz, 1H), 7.70 (dt, J = 10.1, 5.6 Hz, 2H), 7.11 (d, J = 6.2 Hz, 4H), 6.89 (ddd, J = 8.1, 5.9, 1.9 Hz, 1H). ^{13}C NMR (126 MHz, DMSO-d_6) δ 151.91, 143.18, 138.26, 137.40, 135.64, 134.66, 132.61, 129.29, 128.83, 126.06, 124.14, 123.07, 120.18. HRMS (ESI) m/z [M + H]$^{+}$: 285.06530 calcd for $C_{15}H_{12}N_2O_2S$: 285.06833;

N-(o-tolyl)quinoline-8-sulfonamide **(3b)**. White solid, Yield: 63%, m.p. 155.4–157.7 °C. ^{1}H NMR (500 MHz, DMSO) δ 9.23 (s, 1H), 9.17 (dd, J = 4.1, 1.5 Hz, 1H), 8.58 (dd, J = 8.3, 1.4 Hz, 1H), 8.30 (d, J = 8.1 Hz, 1H), 8.24 (d, J = 6.4 Hz, 1H), 7.76 (dd, J = 8.3, 4.2 Hz, 1H), 7.69 (t, J = 7.7 Hz, 1H), 7.07 (d, J = 7.0 Hz, 1H), 7.01–6.91 (m, 2H), 6.85 (d, J = 7.4 Hz, 1H), 2.06 (s, 3H). ^{13}C NMR (126 MHz, DMSO) δ 151.94, 143.19, 137.64, 136.74, 135.84, 134.48, 133.81, 131.62, 131.13, 129.01, 126.67, 126.33, 126.14, 125.13, 123.17, 18.16. HRMS (ESI) m/z [M + H]$^{+}$: 299.08095 calcd for $C_{16}H_{14}N_2O_2S$: 299.08392;

N-(m-tolyl)quinoline-8-sulfonamide **(3c)**. White solid, Yield: 59%, m.p. 161.4–162.9 °C. ^{1}H NMR (500 MHz, DMSO) δ 10.02 (s, 1H), 9.15 (dd, J = 4.2, 1.7 Hz, 1H), 8.51 (dd, J = 8.3, 1.6 Hz, 1H), 8.37 (dd, J = 7.3, 1.1 Hz, 1H), 8.26 (d, J = 8.2 Hz, 1H), 7.77–7.66 (m, 2H), 6.95 (t, J = 7.8 Hz, 1H), 6.89 (s, 1H), 6.83 (d, J = 8.0 Hz, 1H), 6.70 (d, J = 7.5 Hz, 1H), 2.08 (s, 3H). ^{13}C NMR (126 MHz, DMSO) δ 151.91, 143.19, 138.53, 138.18, 137.45, 135.72, 134.66, 132.52, 129.09, 128.85, 126.09, 124.85, 123.09, 120.65, 117.13, 21.45. HRMS (ESI) m/z [M + H]$^{+}$: 299.08095 calcd for $C_{16}H_{14}N_2O_2S$: 299.08389;

N-(p-tolyl)quinoline-8-sulfonamide **(3d)** [48]. Yield: 59%. ^{1}H NMR (500 MHz, DMSO) δ 9.91 (s, 1H), 9.17 (d, J = 3.7 Hz, 1H), 8.50 (d, J = 8.2 Hz, 1H), 8.33 (d, J = 7.2 Hz, 1H), 8.24 (d, J = 8.1 Hz, 1H), 7.82–7.65 (m, 2H), 6.94 (d, J = 7.9 Hz, 2H), 6.88 (d, J = 7.8 Hz, 2H), 2.06 (s, 3H). ^{13}C NMR (126 MHz, DMSO) δ 151.90, 143.17, 137.43, 135.63, 135.53, 134.58, 133.46, 132.52, 129.71, 128.81), 126.08, 123.08, 120.70, 20.62. HRMS (ESI) m/z [M + H]$^{+}$: 299.08095 calcd for $C_{16}H_{14}N_2O_2S$:

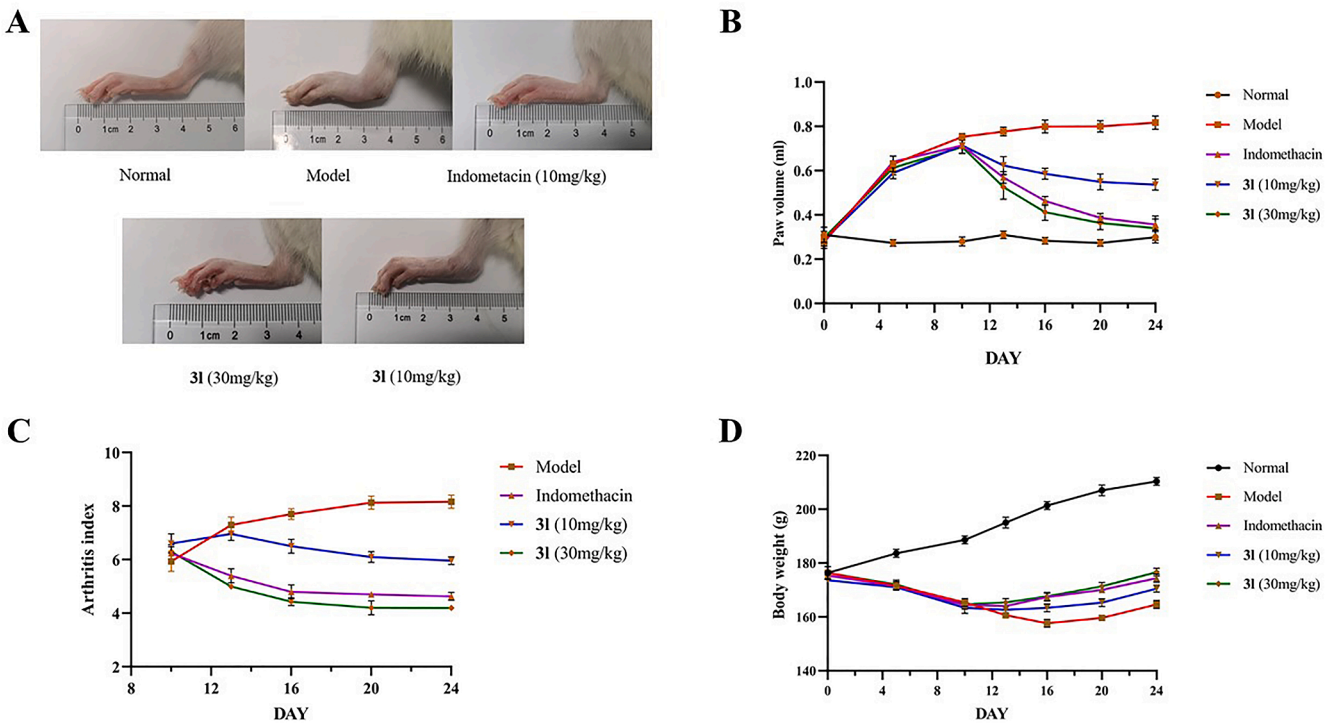

Fig. 9. Effects of compound **3l** on adjuvant-induced arthritic rats. (A) Pictures of treated and untreated feet of rats. (B) Effect of compound **3l** on the body weight of adjuvant-induced arthritic model rats. (C) Effects of compound **3l** on paw swelling in adjuvant-induced arthritic model rats. (D) Effects of compound **3l** on the arthritis index of adjuvant-induced arthritic model rats.

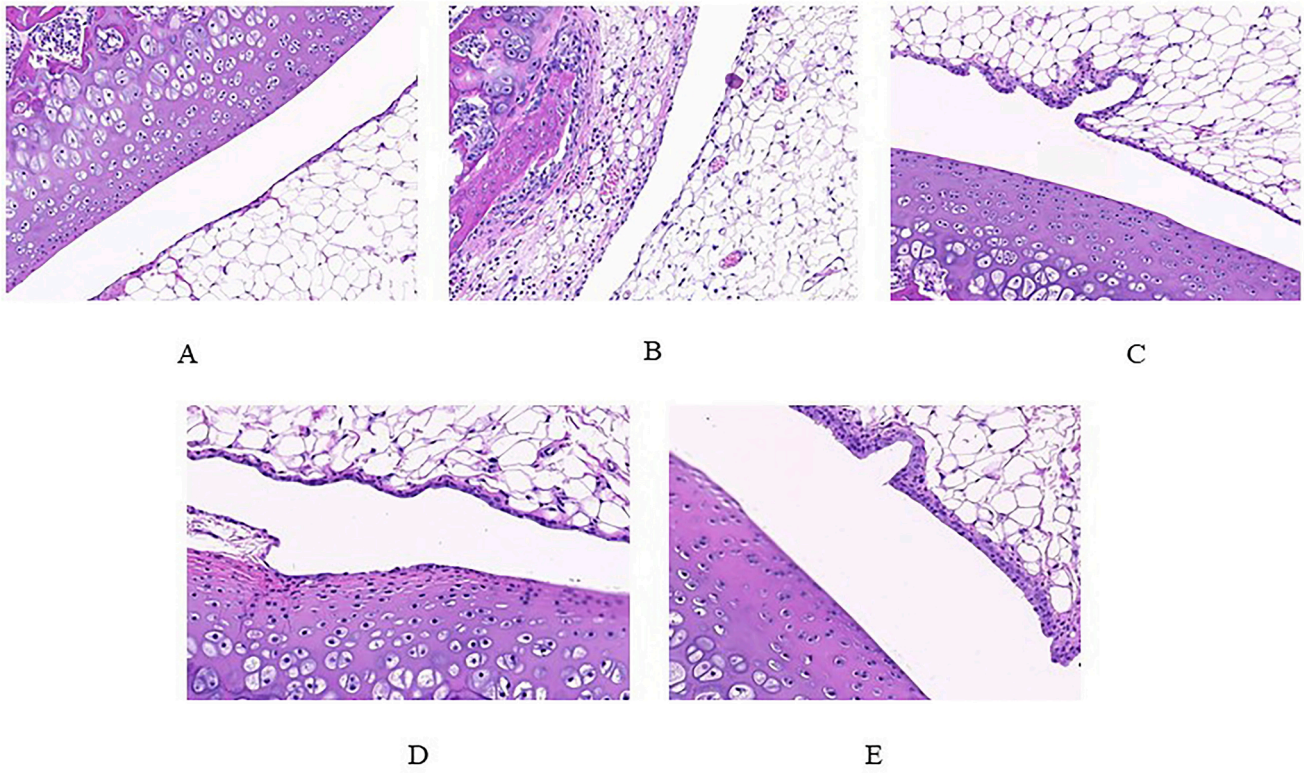

Fig. 10. The effect of compound **3l** on the joint pathological tissue of AIA model rats was explored by HE staining experiment (magnification × 10). (A) Normal; (B) AA; (C) Indometacin 10 mg/kg; (D) Compound **3l**, 30 mg/kg; (E) Compound **3l**, 10 mg/kg.

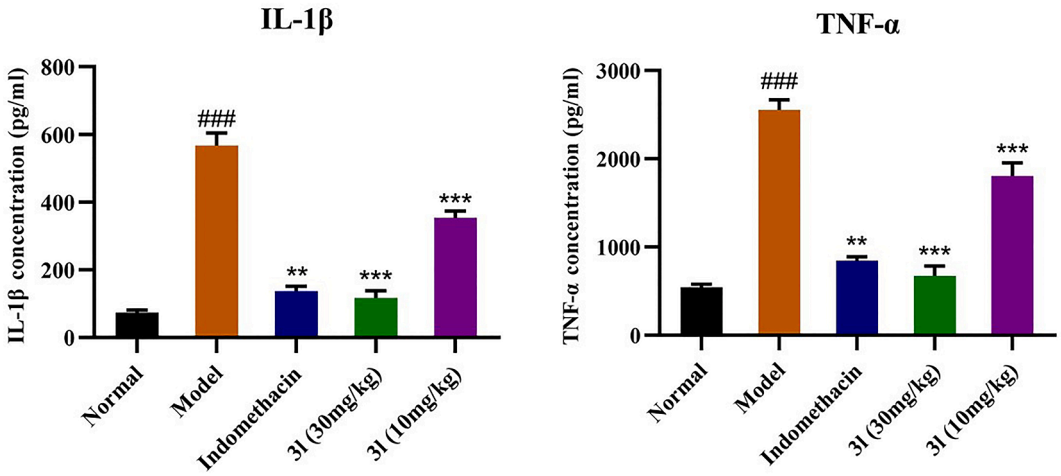

Fig. 11. Inhibitory effects of compound **3l** on inflammatory factors in adjuvant-induced arthritic model rats. (A) Inhibitory effects of compound **3l** on IL-1β production in vivo. (B) Inhibitory effects of compound **3l** on TNF-α production *in vivo*. The results were showed as means ± SD (n = 3) of at least three independent experiments. $^{###}p < 0.0001$ compared with the normal group, $^{**}p < 0.001$, $^{***}p < 0.0001$ compared with the model group.

299.08392;

N-(2-methoxyphenyl)quinoline-8-sulfonamide **(3e)** [49]. Yield: 50%. ^{1}H NMR (500 MHz, DMSO) δ 9.19 (dd, J = 4.1, 1.4 Hz, 1H), 8.95 (s, 1H), 8.56 (dd, J = 8.3, 1.2 Hz, 1H), 8.38–8.22 (m, 2H), 7.77 (dd, J = 8.3, 4.2 Hz, 1H), 7.69 (t, J = 7.7 Hz, 1H), 7.41 (d, J = 7.0 Hz, 1H), 6.96 (t, J = 7.8 Hz, 1H), 6.87–6.72 (m, 2H), 3.31 (s, 3H). ^{13}C NMR (126 MHz, DMSO) δ 151.79, 150.46, 142.91, 137.61, 135.76, 134.66, 131.36, 128.89, 126.48, 125.90, 123.16, 121.86, 121.05, 111.91, 55.77. HRMS (ESI) m/z [M + H]$^+$: 315.07587 calcd for $C_{16}H_{14}N_2O_3S$: 315.07877.

N-(3-methoxyphenyl)quinoline-8-sulfonamide **(3f)**. White solid, Yield: 51%, m.p. 164.8–166.6 °C. ^{1}H NMR (500 MHz, DMSO) δ 10.10 (s, 1H), 9.15 (dd, J = 4.0, 1.4 Hz, 1H), 8.51 (d, J = 7.1 Hz, 1H), 8.39 (d, J = 6.6 Hz, 1H), 8.27 (d, J = 8.0 Hz, 1H), 7.79–7.65 (m, 2H), 6.98 (t, J = 8.4 Hz, 1H), 6.72–6.57 (m, 2H), 6.46 (d, J = 9.7 Hz, 1H), 3.55 (s, 3H). ^{13}C NMR (126 MHz, DMSO) δ 159.85, 151.92, 143.18, 139.42, 137.45, 135.58, 134.76, 132.70, 130.11, 128.86, 126.11, 123.11, 112.15, 108.96, 106.06, 55.30. HRMS (ESI) m/z [M + H]$^+$: 315.07587 calcd for $C_{16}H_{14}N_2O_3S$: 315.07867.

N-(4-methoxyphenyl)quinoline-8-sulfonamide **(3g)** [48]. Yield: 43%. ^{1}H NMR (500 MHz, DMSO) δ 9.72 (s, 1H), 9.19 (dd, J = 4.1, 1.5 Hz, 1H), 8.52 (dd, J = 8.3, 1.3 Hz, 1H), 8.38–8.17 (m, 2H), 7.74 (dd, J = 8.3, 4.2 Hz, 1H), 7.67 (t, J = 7.7 Hz, 1H), 6.93 (d, J = 8.9 Hz, 2H), 6.66 (d, J = 9.0 Hz, 2H), 3.57 (s, 3H). ^{13}C NMR (126 MHz, DMSO) δ 156.72, 151.90, 143.19, 137.48, 135.64, 134.50, 132.38, 130.68, 128.79, 126.11, 123.40, 123.10, 114.45, 55.45. HRMS (ESI) m/z [M + H]$^+$: 315.07587 calcd for $C_{16}H_{14}N_2O_3S$: 315.07880;

N-(2-fluorophenyl)quinoline-8-sulfonamide **(3h)**. White solid, Yield:47%, m.p. 175.4–177.3 °C. ^{1}H NMR (500 MHz, DMSO) δ 9.66 (s, 1H), 9.12 (s, 1H), 8.57 (d, J = 7.1 Hz, 1H), 8.28 (dd, J = 27.4, 6.4 Hz, 2H), 7.91–7.60 (m, 2H), 7.22 (s, 1H), 7.14–6.93 (m, 3H). ^{13}C NMR (126 MHz, DMSO) δ 156.77, 151.86, 143.14, 137.55, 136.18, 134.71, 131.53 , 128.94, 127.40, 126.54, 126.04, 125.25, 124.95, 123.15, 116.26. HRMS (ESI) m/z [M + H]$^+$: 303.05588 calcd for $C_{15}H_{11}FN_2O_2S$: 303.05875;

N-(3-fluorophenyl)quinoline-8-sulfonamide **(3i)**. White solid, Yield: 56%, m.p. 184.4–185.9 °C. ^{1}H NMR (500 MHz, DMSO) δ 10.56 (s, 1H), 9.20 (dd, J = 4.2, 1.7 Hz, 1H), 8.59–8.47 (m, 2H), 8.28 (dd, J = 8.2, 1.2 Hz, 1H), 7.82–7.68 (m, 2H), 7.16 (dd, J = 15.1, 7.9 Hz, 1H), 7.04–6.94 (m, 2H), 6.81–6.64 (m, 1H). ^{13}C NMR (126 MHz, DMSO) δ 163.47, 161.54, 151.97, 143.14, 140.23, 137.41, 135.35, 134.91, 132.85, 130.99, 128.87, 126.07, 123.10, 115.36, 110.47, 110.30, 106.49, 106.29. HRMS (ESI) m/z [M + H]$^+$: 303.05588 calcd for $C_{15}H_{11}FN_2O_2S$: 303.05884;

N-(4-fluorophenyl)quinoline-8-sulfonamide**(3j)**. White solid, Yield: 58%, m.p. 197.4–200.1 °C. ^{1}H NMR (500 MHz, DMSO) δ 10.15 (s, 1H), 9.21 (dd, J = 4.0, 1.4 Hz, 1H), 8.53 (dd, J = 8.3, 1.2 Hz, 1H), 8.39 (d, J = 7.2 Hz, 1H), 8.28 (d, J = 7.9 Hz, 1H), 7.86–7.66 (m, 2H), 7.12 (dd, J = 8.9, 4.9 Hz, 2H), 6.99 (t, J = 8.8 Hz, 2H). ^{13}C NMR (126 MHz, DMSO) δ 160.22, 158.30, 151.94, 143.15, 137.44, 135.43, 134.71, 134.45, 132.58, 128.82, 126.08, 123.10, 122.75, 116.07, 115.89. HRMS (ESI) m/z [M + H]$^+$: 303.05588 calcd for $C_{15}H_{11}FN_2O_2S$: 303.05884;

N-(3,4-difluorophenyl)quinoline-8-sulfonamide **(3k)**. White solid, Yield: 48%, m.p. 174.4–177.1 °C. ^{1}H NMR (500 MHz, DMSO) δ 10.52 (s, 1H), 9.23 (d, J = 2.7 Hz, 1H), 8.53 (dd, J = 28.7, 7.6 Hz, 2H), 8.33 (d, J = 8.0 Hz, 1H), 7.78 (dd, J = 12.3, 5.7 Hz, 2H), 7.21 (ddd, J = 13.3, 9.6, 5.7 Hz, 2H), 6.97 (d, J = 8.9 Hz, 1H). ^{13}C NMR (126 MHz, DMSO) δ 151.99, 143.10, 137.45, 135.17, 134.95, 132.82, 128.86, 126.09, 123.13, 118.13, 117.98, 116.50, 116.43, 109.32, 109.16. HRMS (ESI) m/z [M + H]$^+$: 321.04646 calcd for $C_{15}H_{10}F_2N_2O_2S$: 321.04938;

N-(4-(trifluoromethyl)phenyl)quinoline-8-sulfonamide **(3l)** [50]. Yield: 54%. ^{1}H NMR (500 MHz, DMSO) δ 10.83 (s, 1H), 9.15 (d, J = 2.6 Hz, 1H), 8.51 (dd, J = 11.9, 8.0 Hz, 2H), 8.31 (d, J = 8.0 Hz, 1H), 7.86–7.65 (m, 2H), 7.50 (d, J = 8.5 Hz, 2H), 7.31 (d, J = 8.4 Hz, 2H). ^{13}C NMR (126 MHz, DMSO) δ 152.03, 143.12, 142.20, 137.48, 135.31, 135.10, 132.95, 128.93, 126.69, 126.66, 126.13, 123.18, 118.87. HRMS (ESI) m/z [M + H]$^+$: 353.05269 calcd for $C_{16}H_{11}F_3N_2O_2S$: 353.05542;

N-(4-(trifluoromethoxy)phenyl)quinoline-8-sulfonamide **(3 m)**. White solid, Yield: 51%, m.p. 203.6–205.7 °C. ^{1}H NMR (500 MHz, DMSO) δ 10.43 (s, 1H), 9.16 (dd, J = 4.2, 1.7 Hz, 1H), 8.53 (dd, J = 8.4, 1.6 Hz, 1H), 8.43 (dd, J = 7.3, 1.2 Hz, 1H), 8.29 (dd, J = 8.2, 1.1 Hz, 1H), 7.79–7.66 (m, 2H), 7.26–7.09 (m, 4H). ^{13}C NMR (126 MHz, DMSO) δ 151.97, 144.53, 144.52, 143.14 (s, 1H), 137.54, 137.48, 135.46, 134.89, 132.66, 128.89, 126.12, 123.15, 122.23, 121.33. HRMS (ESI) m/z [M + H]$^+$: 369.04760 calcd for $C_{16}H_{11}F_3N_2O_3S$: 369.05038;

N-(3-chlorophenyl)quinoline-8-sulfonamide **(3n)**. White solid, Yield: 57%, m.p. 189.8–193.2 °C. ^{1}H NMR (500 MHz, DMSO) δ 10.55 (s, 1H), 9.19 (dd, J = 4.2, 1.6 Hz, 1H), 8.56–8.45 (m, 2H), 8.34–8.24 (m, 1H), 7.82–7.69 (m, 2H), 7.21 (d, J = 1.7 Hz, 1H), 7.18–7.08 (m, 2H), 6.99–6.91 (m, 1H). ^{13}C NMR (126 MHz, DMSO) δ 151.99, 143.12, 139.92, 137.43, 135.31, 134.96, 133.57, 132.83, 130.99, 128.87, 126.09, 123.64, 123.12, 119.14, 117.95. HRMS (ESI) m/z [M + H]$^+$: 319.02633 calcd for $C_{15}H_{11}ClN_2O_2S$: 319.02954.

4.3. ADMET prediction

Compounds **3a**–**3n** were introduced into the DS 2017 software, and ADMET descriptors were selected after the compounds were treated. All ADMET parameters, namely, aqueous solubility, BBB penetration,

CYP2D6 binding, hepatotoxicity, and intestinal absorption plasma protein binding, were selected to predict the results.

4.4. Cell culture

Mouse macrophages (RAW264.7 cells, Anhui Medical University) and HEK293T cells (Anhui Medical University) were cultured in DMEM (Hyclone, USA) containing 10% fetal bovine serum, 50 U/ml penicillin, and 50 μg/ml gentamicin and then incubated in an incubator containing 5% CO_2 at 37 °C.

4.5. Cell viability assay

The cytotoxicity of the compounds to RAW264.7 cells was evaluated via MTT assay. RAW264.7 cells (5,000 cells/well) were seeded in a 96-well plate for 24 h (Sigma Aldrich, Australia), and the old medium was discarded. The cells were treated with medium containing the compounds (100, 80, 50, 25, and 12.5 μM) for 24 h and incubated with MTT (5 mg/ml, 20 μL/well) for 4 h. The cell culture supernatants were then discarded, and 150 μL DMSO was added to each well to dissolve formazan. The 96-well plate was placed on a shaker to shake for 10 min, and the absorbance was measured at 492 nm.

4.6. In vitro determination of NO content

RAW264.7 cells (6×10^4 cells per well) were seeded in a 48-well plate for 24 h, and then the medium with different concentrations (100, 60, 40, 20, 10, 5, 2.5, 1.25 and 0.6725 μM) of the compounds was added to continue the culture. After incubation for 1 h, LPS (1 μg/ml, 30 μL/well) was added to stimulate the cells for 24 h. Afterward, 50 μL of the cell culture supernatant was collected and put it into a 96-well plate. Griess Reagent I and Griess Reagent II (50 μL/well) were also added to the 96-well plate to determine the content of NO. After 5 min, the absorbance of the sample was measured at 540 nm.

4.7. In vitro determination of IL-1β and TNF-α content

The steps were similar to those described in Section 4.6. RAW264.7 cells (6×10^4 cells/well) were seeded in 48-well plates. After 24 h, the medium containing different concentrations of the compounds was added for 1 h, and then the cells were added with LPS (1 μg/mL) for 24 h. The content of TNF-α and IL-β in the cell supernatant was measured via ELISA (Jyimei, Wuhan, China) following the manufacturer's instructions.

4.8. Western blot analysis

4.8.1. Antibodies

iNOS was purchased from Zenbio, China (Cat number, 340668, Dilution ratio, 1:1000); COX-2 was purchased from Zenbio, China (Cat number, 383971, Dilution ratio, 1:1000); Actin was purchased from Beyotime, China (Cat number, AF5003, Dilution ratio, 1:5000); IκB was purchased from Beyotime, China (Cat number, AF1282, Dilution ratio, 1:2000); p-IκB was purchased from Beyotime, China (Cat number, AF1870, Dilution ratio, 1:1000); P65 was purchased from Zenbio, China (Cat number, 380172, Dilution ratio, 1:5000); p-P65 was purchased from Zenbio, China (Cat number, 310012, Dilution ratio, 1:1000); P38 was purchased from Zenbio, China (Cat number, R25239, Dilution ratio, 1:1000); p-P38 was purchased from Zenbio, China (Cat number, 310091, Dilution ratio, 1:1000); ERK was purchased from Zenbio, China (Cat number, 343830, Dilution ratio, 1:1000); p-ERK was purchased from Zenbio, China (Cat number, 301245, Dilution ratio, 1:1000); JNK was purchased from Zenbio, China (Cat number, 310012, Dilution ratio, 1:1000); p-JNK was purchased from Zenbio, China (Cat number, 310012, Dilution ratio, 1:1000); secondary antibody was purchased from Zenbio, China (Cat number, 550064, Dilution ratio, 1:10000).

4.8.2. General procedure

RAW264.7 cells (3×10^5 cells/well) were seeded in 6-well plates and incubated for 24 h. The cells were pretreated with compound **3l** (1, 3, and 10 μM) for 1 h and then stimulated with LPS (1 μg/mL) for 24 h. After washing the cells with 1 × PBS, 300 μL of cell lysis buffer (RIRA lysis buffer, phosphatase inhibitor, protease inhibitor, and PMSF) was added to each well, incubated on ice for 30 min, and then centrifuged at 12,000 r/min for 30 min at 4 °C to collect the supernatant. Protein content was determined using a protein quantification kit (BCA Assay, Beyotime, Shanghai, China). Total proteins were separated by 10% SDS-PAGE and then transferred from the gel to a PVDF membrane (Millipore, Sigma). The membranes were blocked in TBST solution containing 5% skimmed milk for 2 h. Afterward, the membranes were washed three times (TBST) and incubated with the primary antibody dilution overnight at 4 °C. After washing three times with TBST, the membranes were combined with the corresponding diluted secondary antibody for 90 min at room temperature. The blots were visualized by a chemiluminescence imager (Tanon 5200, Shanghai, China).

4.9. Target fishing and molecular docking

The potential drug targets of compound **3l** were predicted and screened using the DS 2017 software. The structure of compound **3l** (ligand) was drawn using the Chemdraw 2017 software and imported into the DS software. After the ligand was prepared and the energy was minimized, the potential targets of the compounds were virtually screened through the *Ligand Profiler* program in the DS software. The results were analyzed according to the fit value of the binding between the ligand and each protein (the higher the fit value was, the better compound **3l** matched the corresponding protein). The target corresponding to the protein was the likely target of the compound. For further analysis, compound **3l** and adenosine kinase protein were combined through CDOCKER molecular docking.

4.10. Co-immunoprecipitation

After 30 min of pretreatment with **3l** of 30 μM, RAW264.7 cells were stimulated by LPS for 15 min. The cells were lysed by adding buffer (Cell lysis buffer for Western and IP, PMSF), and the cell lysate was collected. The cell extracts were incubated with an appropriate amount of anti-MD2 antibody (Cat number, 822065, Dilution ratio, 1:1000, Zenbio, China) and precipitated with A + G agarose beads (Beyotime, China) overnight at 4 °C. After boiling, the released protein was detected by immunoblot using anti-TLR4 antibody (Cat number, 505208, Dilution ratio, 1:1000, Zenbio, China).

HEK293T cells were seeded at 4×10^5 cells/dish in a 6-well plate overnight and then co-transfected with HA-TLR4 (3 μg) and Flag-TLR4 (3 μg) plasmids for 24 h. Afterward, the cells were seeded at 4×10^5 in a 5 cm (i.d.) dish and cultured for 24 h. The cells were pretreated with compound **3l** for 1 h and cultured with LPS (1 mg/mL) treatment 12 h. The IP lysis buffer (Cell lysis buffer for Western and IP, PMSF) was added to the Petri dish to harvest the cells. The effect of compound **3l** on the formation of TLR4 dimers was analyzed by Western blot and anti-HA magnetic beads.

4.11. Cellular thermal shift assay

RAW264.7 cells were seeded in a 6-well plate for 24 h (6×10^4 cells/well). After the cells were treated with compound **3l** (30 μM) for 12 h, the protein was collected with cell lysate. The protein was then evenly divided into four parts and heated at different temperatures (45 °C, 50 °C, 55 °C, 60 °C and 65 °C) for 3 min. The results were analyzed by Western blot.

4.12. In vivo experiment

4.12.1. Animals

Sprague–Dawley female rats weighing 160–180 g were purchased from the Animal Experiment Center of Anhui University of Chinese Medicine. The temperature, relative humidity, and dark–light cycle per day of the animal room was maintained at 23 °C–25 °C, 40%–60%, and 12 h, respectively. The animal experiments were approved by the Experimental Animal Ethics Committee of Anhui Medical University.

4.12.2. Induction of adjuvant arthritis and experimental design

The rats were injected with 0.1 mL Freund's adjuvant complete (FCA) intracutaneously into the left hind feet to cause inflammation. The rats in the normal group were injected with the same amount of physiological saline at the same site.

The rats were randomly divided into four groups after 10 days of FCA injection. The two groups were treated with compound **3l** (10 and 30 mg/kg) for 14 days, and the rats in the positive control group were treated with indomethacin (10 mg/kg) for 14 days.

4.12.3. HE staining

The inflamed contralateral knee joints of the rats were removed, kept in 4% paraformaldehyde solution, decalcified with 5% formic acid, and then embedded in paraffin. The sections were stained with HE. Histopathological changes were observed under an optical microscope.

4.12.4. In vivo determination of IL-1β, and TNF-α content

After the rats were anesthetized, blood was collected from the heart artery. It was allowed to stand for 30 min. The blood sample was centrifuged at 3000 r/min for 10 min at 4 °C to collect the serum. The serum levels of IL-1β, and TNF-α were determined via ELISA.

4.12.5. Statistical analysis

Data are reported as mean ± SEM of at least three independent experiments and data analysis was performed with GraphPad Prism 8 software.

Declaration of Competing Interest

The authors declare that they have no known competing financial interests or personal relationships that could have appeared to influence the work reported in this paper.

Acknowledgments

We thank the Excellent Young Talents Fund Program of Higher Education Institutions of Anhui Province (CN) (gxyq202006), the Natural Science Research Project of the Educational Commission of Anhui Province of China (KJ2019A0231) and the basic health research project in Anhui Province (GXXT-2019-045) for financial support of this study. We also thank the Center for Scientific Research of Anhui Medical University for valuable help in our experiment.

Appendix A. Supplementary material

Supplementary data to this article can be found online at https://doi.org/10.1016/j.bioorg.2021.105037.

References

[1] J. Chen, D.L. Li, L.N. Xie, Y.R. Ma, P.P. Wu, C. Li, W.F. Liu, K. Zhang, R.P. Zhou, X. T. Xu, X. Zheng, X. Liu, Synergistic anti-inflammatory effects of silibinin and thymol combination on LPS-induced RAW264.7 cells by inhibition of NF-kappaB and MAPK activation, Phytomedicine 78 (2020), 153309.

[2] Y.L. Tang, X. Zheng, Y. Qi, X.J. Pu, B. Liu, X. Zhang, X.S. Li, W.L. Xiao, C.P. Wan, Z. W. Mao, Synthesis and anti-inflammatory evaluation of new chalcone derivatives bearing bispiperazine linker as IL-1beta inhibitors, Bioorg. Chem. 98 (2020), 103748.

[3] L.Z. Chen, W.W. Sun, L. Bo, J.Q. Wang, C. Xiu, W.J. Tang, J.B. Shi, H.P. Zhou, X. H. Liu, New arylpyrazoline-coumarins: Synthesis and anti-inflammatory activity, Eur. J. Med. Chem. 138 (2017) 170–181.

[4] R. Medzhitov, Origin and physiological roles of inflammation, Nature 454 (2008) 428–435.

[5] A. Linde, D. Mosier, F. Blecha, T. Melgarejo, Innate immunity and inflammation–New frontiers in comparative cardiovascular pathology, Cardiovasc. Res. 73 (2007) 26–36.

[6] L.F. Shirazi, J. Bissett, F. Romeo, J.L. Mehta, Role of Inflammation in Heart Failure, Curr. Atheroscler. Rep 19 (2017) 27.

[7] C. Bogdan, Nitric oxide and the immune response, Nat. Immunol. 2 (2001) 907–916.

[8] R. Heiran, S. Sepehri, A. Jarrahpour, C. Digiorgio, H. Douafer, J.M. Brunel, A. Gholami, E. Riazimontazer, E. Turos, Synthesis, docking and evaluation of in vitro anti-inflammatory activity of novel morpholine capped beta-lactam derivatives, Bioorg. Chem. 102 (2020), 104091.

[9] Y.H. Seo, J.K. Kim, J.G. Jun, Synthesis and biological evaluation of piperlongumine derivatives as potent anti-inflammatory agents, Bioorg. Med. Chem. Lett. 24 (2014) 5727–5730.

[10] J. Li, X. Fan, J. Deng, Y. Liang, S. Ma, Y. Lu, J. Zhang, T. Shi, W. Tan, Z. Wang, Design and synthesis of 1,3-benzothiazinone derivatives as potential anti-inflammatory agents, Bioorg. Med. Chem. 28 (2020), 115526.

[11] S. Sehajpal, D.N. Prasad, R.K. Singh, Prodrugs of Non-steroidal Anti-inflammatory Drugs (NSAIDs): A Long March Towards Synthesis of Safer NSAIDs, Mini Rev. Med. Chem. 18 (2018) 1199–1219.

[12] Y. Xu, S. Chen, Y. Cao, P. Zhou, Z. Chen, K. Cheng, Discovery of novel small molecule TLR4 inhibitors as potent anti-inflammatory agents, Eur. J. Med. Chem. 154 (2018) 253–266.

[13] U. Debnath, S. Mukherjee, N. Joardar, S.P. Sinha Babu, K. Jana, A.K. Misra, Aryl quinolinyl hydrazone derivatives as anti-inflammatory agents that inhibit TLR4 activation in the macrophages, Eur. J. Pharm. Sci. 134 (2019) 102–115.

[14] H.J. Chung, W. Koh, W.K. Kim, J.S. Shin, J. Lee, S.K. Lee, I.H. Ha, The anti-inflammatory effects of Shinbaro3 Is mediated by downregulation of the TLR4 signalling pathway in LPS-stimulated RAW 264.7 macrophages, Mediators Inflamm. 2018 (2018), 4514329.

[15] H. Gao, N. Kang, C. Hu, Z. Zhang, Q. Xu, Y. Liu, S. Yang, Ginsenoside Rb1 exerts anti-inflammatory effects in vitro and in vivo by modulating toll-like receptor 4 dimerization and NF-kB/MAPKs signaling pathways, Phytomedicine 69 (2020), 153197.

[16] X.Z. Han, R. Ma, Q. Chen, X. Jin, Y.Z. Jin, R.B. An, X.M. Piao, M.L. Lian, L.H. Quan, J. Jiang, Anti-inflammatory action of Athyrium multidentatum extract suppresses the LPS-induced TLR4 signaling pathway, J. Ethnopharmacol. 217 (2018) 220–227.

[17] H. Ju Woo, D.Y. Jun, J.Y. Lee, H.S. Park, M.H. Woo, S.J. Park, S.C. Kim, C.H. Yang, Y.H. Kim, Anti-inflammatory action of 2-carbomethoxy-2,3-epoxy-3-prenyl-1,4-naphthoquinone (CMEP-NQ) suppresses both the MyD88-dependent and TRIF-dependent pathways of TLR4 signaling in LPS-stimulated RAW264.7 cells, J. Ethnopharmacol. 205 (2017) 103–115.

[18] Y. Zhang, C. Liu, B. Dong, X. Ma, L. Hou, X. Cao, C. Wang, Anti-inflammatory activity and mechanism of surfactin in lipopolysaccharide-activated macrophages, Inflammation 38 (2015) 756–764.

[19] Z. Liu, L. Chen, P. Yu, Y. Zhang, B. Fang, C. Wu, W. Luo, X. Chen, C. Li, G. Liang, Discovery of 3-(Indol-5-yl)-indazole derivatives as novel myeloid differentiation protein 2/toll-like receptor 4 antagonists for treatment of acute lung injury, J. Med. Chem. 62 (2019) 5453–5469.

[20] S.A. Chavez, A.J. Martinko, C. Lau, M.N. Pham, K. Cheng, D.E. Bevan, T.E. Mollnes, H. Yin, Development of beta-amino alcohol derivatives that inhibit Toll-like receptor 4 mediated inflammatory response as potential antiseptics, J. Med. Chem. 54 (2011) 4659–4669.

[21] W. Karunarathne, K.T. Lee, Y.H. Choi, C.Y. Jin, G.Y. Kim, Anthocyanins isolated from Hibiscus syriacus L. attenuate lipopolysaccharide-induced inflammation and endotoxic shock by inhibiting the TLR4/MD-2-mediated NF-kappaB signaling pathway, Phytomedicine 76 (2020), 153237.

[22] A. Marella, O.P. Tanwar, R. Saha, M.R. Ali, S. Srivastava, M. Akhter, M. Shaquiquzzaman, M.M. Alam, Quinoline: A versatile heterocyclic, Saudi Pharm. J. 21 (2013) 1–12.

[23] C.H. Tseng, C.W. Tung, C.H. Wu, C.C. Tzeng, Y.H. Chen, T.L. Hwang, Y.L. Chen, Discovery of Indeno[1,2-c]quinoline derivatives as potent dual antituberculosis and anti-inflammatory agents, Molecules 22 (2017).

[24] I. Chaaban, O.H. Rizk, T.M. Ibrahim, S.S. Henen, E.M. El-Khawass, A.E. Bayad, I. M. El-Ashmawy, H.A. Nematalla, Synthesis, anti-inflammatory screening, molecular docking, and COX-1,2/-5-LOX inhibition profile of some novel quinoline derivatives, Bioorg. Chem. 78 (2018) 220–235.

[25] P. Gao, L. Wang, L. Zhao, Q.Y. Zhang, K.W. Zeng, M.B. Zhao, Y. Jiang, P.F. Tu, X. Y. Guo, Anti-inflammatory quinoline alkaloids from the root bark of Dictamnus dasycarpus, Phytochemistry 172 (2020), 112260.

[26] X.F. Shang, S.L. Morris-Natschke, G.Z. Yang, Y.Q. Liu, X. Guo, X.S. Xu, M. Goto, J. C. Li, J.Y. Zhang, K.H. Lee, Biologically active quinoline and quinazoline alkaloids part II, Med. Res. Rev. 38 (2018) 1614–1660.

[27] H. Suleyman, E. Cadirci, A. Albayrak, Z. Halici, Nimesulide is a selective COX-2 inhibitory, atypical non-steroidal anti-inflammatory drug, Curr. Med. Chem. 15 (2008) 278–283.

[28] Vinod Kumar, Kamalneet Kaura, Girish K. Gupta, Akhilesh K. Guptaa, S. Kumar, Developments in synthesis of the anti-inflammatory drug, celecoxib: a review, Recent Pat. Inflamm. Allergy Drug Discov. 7 (2013) 124–134.
[29] Y. Sun, Q. Xu, Z. Wu, Y. Gong, L. Tang, Parecoxib inhibits inflammatory responses in a mouse model of sepsis, FEBS Open Biol. (2020).
[30] M. Wu, J. Ma, L. Ji, M. Wang, J. Han, Z. Li, Design, synthesis, and biological evaluation of rutacecarpine derivatives as multitarget-directed ligands for the treatment of Alzheimer's disease, Eur. J. Med. Chem. 177 (2019) 198–211.
[31] J. Grover, V. Kumar, V. Singh, K. Bairwa, M.E. Sobhia, S.M. Jachak, Synthesis, biological evaluation, molecular docking and theoretical evaluation of ADMET properties of nepodin and chrysophanol derivatives as potential cyclooxygenase (COX-1, COX-2) inhibitors, Eur. J. Med. Chem. 80 (2014) 47–56.
[32] L. Ma, H. Pei, L. Lei, L. He, J. Chen, X. Liang, A. Peng, H. Ye, M. Xiang, L. Chen, Structural exploration, synthesis and pharmacological evaluation of novel 5-benzylidenethiazolidine-2,4-dione derivatives as iNOS inhibitors against inflammatory diseases, Eur. J. Med. Chem. 92 (2015) 178–190.
[33] L.Z. Chen, J. Wu, K. Li, Q.Q. Wu, R. Chen, X.H. Liu, B.F. Ruan, Novel phthalide derivatives: Synthesis and anti-inflammatory activity in vitro and in vivo, Eur. J. Med. Chem. 206 (2020), 112722.
[34] W. Fan, F. Huang, C. Li, H. Qu, Z. Gao, S. Leng, D. Li, H. He, Involvement of NOS/NO in the development of chronic dental inflammatory pain in rats, Brain Res. Rev. 59 (2009) 324–332.
[35] T. Sogo, N. Terahara, A. Hisanaga, T. Kumamoto, T. Yamashiro, S. Wu, K. Sakao, D. X. Hou, Anti-inflammatory activity and molecular mechanism of delphinidin 3-sambubioside, a Hibiscus anthocyanin, BioFactors 41 (2015) 58–65.
[36] M. Wang, T. Liu, S. Chen, M. Wu, J. Han, Z. Li, Design and synthesis of 3-(4-pyridyl)-5-(4-sulfamido-phenyl)-1,2,4-oxadiazole derivatives as novel GSK-3beta inhibitors and evaluation of their potential as multifunctional anti-Alzheimer agents, Eur. J. Med. Chem. 209 (2021), 112874.
[37] H.N. Kim, J.D. Kim, J.H. Yeo, H.J. Son, S.B. Park, G.H. Park, H.J. Eo, J.B. Jeong, Heracleum moellendorffii roots inhibit the production of pro-inflammatory mediators through the inhibition of NF-kappaB and MAPK signaling, and activation of ROS/Nrf2/HO-1 signaling in LPS-stimulated RAW264.7 cells, BMC Complement Altern. Med. 19 (2019) 310.
[38] H. Huang, G. Zhang, Y. Zhou, C. Lin, S. Chen, Y. Lin, S. Mai, Z. Huang, Reverse screening methods to search for the protein targets of chemopreventive compounds, Front. Chem. 6 (2018) 138.
[39] D. Carvalho, M. Paulino, F. Polticelli, F. Arredondo, R.J. Williams, J.A. Abin-Carriquiry, Structural evidence of quercetin multi-target bioactivity: A reverse virtual screening strategy, Eur. J. Pharm. Sci. 106 (2017) 393–403.
[40] T. Kawai, S. Akira, Toll-like receptor downstream signaling, Arthritis Res. Ther. 7 (2005) 12–19.
[41] J. Perrin, T. Werner, N. Kurzawa, A. Rutkowska, D.D. Childs, M. Kalxdorf, D. Poeckel, E. Stonehouse, K. Strohmer, B. Heller, D.W. Thomson, J. Krause, I. Becher, H.C. Eberl, J. Vappiani, D.C. Sevin, C.E. Rau, H. Franken, W. Huber, M. Faelth-Savitski, M.M. Savitski, M. Bantscheff, G. Bergamini, Identifying drug targets in tissues and whole blood with thermal-shift profiling, Nat. Biotechnol. 38 (2020) 303–308.
[42] Lingyun Dai, Nayana Prabhu, Liang Ying Yu, Smaranda Bacanu, Anderson Daniel Ramos, P. Nordlund, Horizontal cell biology: monitoring global changes of protein interaction states with the proteome-wide cellular thermal shift assay (CETSA), Annu. Rev. Biochem. 88 (2019) 383–408.
[43] F.B. Reinhard, D. Eberhard, T. Werner, H. Franken, D. Childs, C. Doce, M. F. Savitski, W. Huber, M. Bantscheff, M.M. Savitski, G. Drewes, Thermal proteome profiling monitors ligand interactions with cellular membrane proteins, Nat. Methods 12 (2015) 1129–1131.
[44] J.M. Dziekan, G. Wirjanata, L. Dai, K.D. Go, H. Yu, Y.T. Lim, L. Chen, L.C. Wang, B. Puspita, N. Prabhu, R.M. Sobota, P. Nordlund, Z. Bozdech, Cellular thermal shift assay for the identification of drug-target interactions in the Plasmodium falciparum proteome, Nat. Protoc. 15 (2020) 1881–1921.
[45] L.Z. Chen, L. Yao, M.M. Jiao, J.B. Shi, Y. Tan, B.F. Ruan, X.H. Liu, Novel resveratrol-based flavonol derivatives: Synthesis and anti-inflammatory activity in vitro and in vivo, Eur. J. Med. Chem. 175 (2019) 114–128.
[46] E. Choi, J. Lee, S. Lee, B.W. Song, H.H. Seo, M.J. Cha, S. Lim, C. Lee, S.W. Song, G. Han, K.C. Hwang, Potential therapeutic application of small molecule with sulfonamide for chondrogenic differentiation and articular cartilage repair, Bioorg. Med. Chem. Lett. 26 (2016) 5098–5102.
[47] K.-T. Hsu, Internal Marketing Based on the Hierarchy of Effects Model for the Life Insurance Industry, Int. Bus. Res. 9 (2016) 1.
[48] N.M. Vinokurova, I.K. Fel'dman, Synthesis and properties of some sulfonamides of the quinoline series Pharmaceutical, Chemistry 10 (1968) 34–36.
[49] David Scott Goldfarb, Method for altering the lifespan of eukaryotic organisms in: U.S. Pat (Ed.), US, 2009.
[50] M.M.V. RAMANA, R.S. LOKHANDE, G. GAYATRIVIJAY, A process for the synthesis of sulfonamide derivatives and their antituberculosis activity., in: U.S. Pat (Ed.), US, 2002.